ARTICLES

Hydrogen Evolution on Supported Incomplete Cubane-type $[Mo_3S_4]^{4+}$ Electrocatalysts

Thomas F. Jaramillo,[†] Jacob Bonde,[‡] Jingdong Zhang,[§] Bee-Lean Ooi,[§] Klas Andersson,[‡] Jens Ulstrup,[§] and Ib Chorkendorff*,[‡]

Department of Chemical Engineering, Stanford University, 381 North-South Mall, Stauffer III, Stanford, California 94305-5025, USA and Center for Individual Nanoparticle Functionality (CINF), Department of Physics; and Department of Chemistry, Technical University of Denmark, DK-2800 Lyngby, Denmark

Received: March 28, 2008; Revised Manuscript Received: June 5, 2008

Electrocatalytic properties of biomimetic supported incomplete cubane-type $[Mo_3S_4]^{4+}$ clusters are investigated. The activity toward the hydrogen evolution reaction (HER) is evaluated on both a high surface area gas diffusion electrode in a membrane electrode assembly and on highly orientated pyrolytic graphite (HOPG) supports. Sub-monolayers of the clusters were imaged by means of scanning tunnelling microscopy (STM) prior to electrochemical characterization. This enabled the quantification of the activity on a per cluster basis for the HER and the comparison of the activity with other HER catalysts. We find that the HER activity of the $[Mo_3S_4]^{4+}$ is comparable with that of the edge sites of MoS_2. The supported $[Mo_3S_4]^{4+}$ molecules were also characterized by X-ray photoelectron spectroscopy (XPS), and the observed deterioration in electrocatalytic activity with time was assigned to slow $[Mo_3S_4]^{4+}$ cathodic desorption from the catalyst support.

1. Introduction

Interfacial electrocatalytic charge transfer processes are at the heart of future energy conversion. Decades of research into conventional metals and alloys have paved the way for the development of the electrocatalytic materials used in today's commercial devices, including fuel cells and electrolyzers.[1] A number of challenges, however, remain in developing active, stable, and low-cost catalysts. Sulfur-rich transition metal clusters have attracted much attention due to their inherently interesting chemistry and their structural and functional relevance to redox metalloproteins and metalloenzymes.[2−11] The latter observations offer particular perspectives for the potential use of such clusters in heterogeneous catalysis and interfacial electrocatalysis.

Monolayers of a variety of redox metalloenzymes in protein film voltammetry can be brought to retain electrocatalytic electron transfer and redox enzyme function in the immobilized state on, usually modified, electrode surfaces. These enzymes include iron−sulfur cluster-based enzymes as well as Mo−enzymes in processes such as fumarate reduction and succinate oxidation, nitrate reduction, dimethyl sulfoxide (DMSO) reduction, and, particularly, hydrogen evolution and proton reduction.[12−14] Although of great importance, redox metalloenzyme function is, however, unlikely to carry over as large-scale industrial electrocatalysts. This is due to their high cost and fragile nature in non-native surroundings outside their natural biological environments. Even though the individual enzyme molecule may be catalytically highly active, the large size of the molecules also means that the number of enzyme molecular sites on the surface in a full monolayer is much smaller than the number of active sites on metallic catalytic surfaces.

Biomimetic electrocatalysts based on chemically synthesized low-cost, earth-abundant metal-containing groups that resemble the active core groups in redox metalloenzymes may, on the other hand, be able to retain electrocatalytic activity at a small size. The heme group as the core group in a broad variety of heme proteins is an example of such a robust and catalytically specific molecular electrocatalyst.[15−19] Synthetic iron−sulfur cubane-like structures resembling the core metal centers in iron−sulfur proteins and metalloenzymes have also been extensively studied by Holm and associates.[2−5] These are, however, fragile and difficult to handle, and they have not been addressed with a view on interfacial electrocatalysis.

Polynuclear sulfide-containing Mo-complexes instead offer a class of robust and relatively easier-to-handle homologues to the iron−sulfur cubane-type clusters The trimeric, incomplete cubane-type cluster aqua ion, $[Mo_3S_4(H_2O)_9]^{4+}$ ($[Mo_3S_4]^{4+}$), in particular, has been extensively investigated,[5] see Figure 1. $[Mo_3S_4]^{4+}$ is extremely stable but is electrochemically reactive, and when coordinated to ligands such as iminodiacetate, evidence for three different oxidation states has been obtained.[6] This suggests that its electrocatalytic activity may be promising. $[Mo_3S_4]^{4+}$ reacts readily with a range of metals or metal ions to form heterometallic complete cubane-type clusters, $[Mo_3MS_4]^{n+}$ (M = Pd, Pt, Ru, Ni, Fe, etc.), thus offering possibilities for tuning of the redox potential and other catalytically important properties. Several of these heterometallic cubane-type $[Mo_3MS_4]^{n+}$ clusters appeared to be catalytically active, for example, in hydrazine N−N cleavage reactions,[7] lactonization of alkynoic acids,[8] hydrodesulfurization,[9] and other organic chemical reactions.[10] The recently reported spontaneous adsorption of $[Mo_3S_4]^{4+}$ on Au(111) surfaces resulting in

* Corresponding author e-mail: ibchork@fysik.dtu.dk; phone: (45) 4525 3170; fax: (45) 4593 2399.
[†] Stanford University.
[‡] Center for Individual Nanoparticle Functionality (CINF), Department of Physics, Technical University of Denmark.
[§] Department of Chemistry, Technical University of Denmark.

10.1021/jp802695e CCC: $40.75
Published on Web 10/17/2008

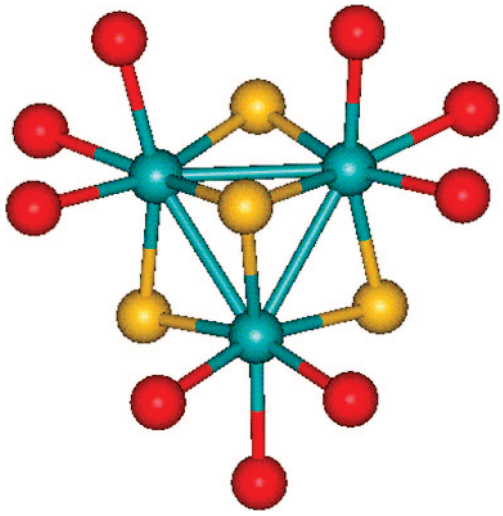

Figure 1. Molecular structure of $[Mo_3S_4]^{4+}$. Blue (Mo), yellow (S), and red (O from water ligands).

$[Mo_3S_4]^{4+}$-monolayer formation[11] is also noteworthy. It is the first example of monolayer formation in situ by a polynuclear metal−sulfide cluster directly anchored onto the gold surface and structurally mapped to single-molecule resolution by scanning tunnelling microscopy directly in aqueous electrolyte solution (in situ STM). Coupled with the different accessible redox-states for polynuclear metal−sulfide clusters, this has sparked off the idea of exploiting the $[Mo_3S_4]^{4+}$ for functionalization of other materials.

We report here comprehensive data for supported incomplete cubane-type $[Mo_3S_4]^{4+}$ as an intriguing new class of materials that holds promise for efficient electrocatalysis of one of the altogether most important electrochemical processes, the electrochemical hydrogen evolution reaction (HER). Flexibility in cluster synthesis, composition, and structure may allow for new electrode materials to be tailored based on these relatively low-cost, earth-abundant elements. We provide voltammetric current−overpotential relations on carbon-supported (high surface area carbon and highly oriented pyrolytic graphite, HOPG) multi- and monolayers of the $[Mo_3S_4]^{4+}$ molecules. STM of the cluster molecules on activated HOPG that "resemble" the high surface area carbon, resolved to the level of the single molecule, enables further direct comparison between the macroscopic electrochemical exchange currents and the density of molecules on the surface. Catalytic activity per molecule can be estimated in this way. Comprehensive electronic characterization of different states of the $[Mo_3S_4]^{4+}$ molecules using X-ray photoelectron spectroscopy (XPS) has finally been achieved.

Models of catalysis that allow us to understand catalytic reactions at a molecular level have emerged in recent years.[20,21] By carefully examining the active site of working systems, we can identify the material (or site) properties that principally control electrocatalytic activity and then search for other, less expensive, systems that emulate these properties. As noted, the HER is an important interfacial electrochemical process that could have a crucial role in a future hydrogen economy.[22] In 1958, Parsons[23] first proposed the descriptor for facile hydrogen evolution, that is, thermoneutral H-adsorption from electrochemical reduction of the solute proton. Optimal catalytic surfaces are those that exhibit a Gibbs free energy of electrochemical H-adsorption (ΔG_H) close to zero, a notion that has recently gained much more attention. Recent DFT calculations have shown that there is indeed a correlation between calculated values of ΔG_H and experimentally measured exchange current densities on a wide range of materials.[24−27]

In approaching catalytic materials discovery, we have previously aimed to emulate enzymatic catalysis using solid-state materials.[27,28] The edge sites of nanoparticulate MoS_2 mimics, in many ways, the metallic active sites in the nitrogenase and hydrogenase enzymes, both of which evolve hydrogen from protons in a facile manner without the use of precious metals.[27,28] Structurally speaking, the primary commonality between the enzymatic active center and the MoS_2 edge is undercoordinated sulfur, which in both cases was shown to be the active site for the HER,[27] as determined by DFT calculations.[28] The $[Mo_3S_4]^{4+}$ studied herein also exhibits this structural commonality, inspiring further study of electrocatalytic reactions, and the HER in particular.

The incomplete cubane-type $[Mo_3S_4]^{4+}$ was first synthesized nearly two decades ago,[6] but studies of electrocatalytic activity have not been reported before. In this report we present data for the electro-catalytic activity of $[Mo_3S_4]^{4+}$ on a high surface area carbon support (Vulcan xc72) followed by a more detailed study of the adsorption and electrocatalytic activity of individually separated $[Mo_3S_4]^{4+}$ molecules supported onto HOPG surfaces. By combining electrochemistry with surface science techniques, we have investigated and assessed this new class of biomimetic, solid-state electrocatalysts.

2. Experimental Methods

2.1. Synthesis of $[Mo_3S_4]^{4+}$. $[Mo_3S_4]^{4+}$ was synthesized by reduction of either ammonium tetrathiomolybdate or the $Mo(V)_2$ aqua ion, $[Mo_2O_2S_2(H_2O)_6]^{2+}$, with sodium borohydride, as reported in the literature.[29,30] Solutions of $[Mo_3S_4]^{4+}$ in H_2SO_4 were obtained by repeated cation-exchange chromatography (Dowex 50W-X2, 400 mesh) and checked by UV−vis spectroscopy (Hewlett-Packard 8453).

2.2. $[Mo_3S_4]^{4+}$-electrode Preparation. Phosphate buffer (PB) solutions were prepared from Suprapur chemicals, dipotassium hydrogen phosphate (K_2HPO_4, 99.99%) and potassium dihydrogen phosphate (KH_2PO_4, 99.995%). The $[Mo_3S_4]^{4+}$/HOPG samples were prepared in two different ways. One is to directly cast a drop (50 μL) of $[Mo_3S_4]^{4+}$ solution (1.8 mM of $[Mo_3S_4]^{4+}$ in 0.4 M H_2SO_4) onto a freshly cleaved HOPG surface. Physical adsorption is the main interaction between the adsorbate and HOPG surface in this procedure. The drop was allowed to dry in a desiccator, and the sample was used as such after a single rinse with a drop of water. This simple method works efficiently with hydrophobic molecules for which hydrophobic interactions are the driving force in stable adlayer formation. However, a stable adlayer for hydrophilic molecules cannot easily be maintained in this way. The HOPG surface must first be activated into a hydrophilic form compatible with a hydrophilic adsorbate such as $[Mo_3S_4]^{4+}$. In the second method, the HOPG was thus activated prior to drop-casting. The activation of HOPG was carried out in pH 7.0 PB solution by the electrochemical method in ref 31. Immediately after activation and rinsing, a freshly prepared 50 μL aliquot of 1.8 mM $[Mo_3S_4]^{4+}$ in 0.4 M H_2SO_4 (aq) was drop-casted onto the activated HOPG surface and soaked for 2 h. Excess solution was washed away by thorough rinsing with Millipore water (18.2 MΩ cm).

2.3. Electrochemical Measurements in a Three-electrode Cell. Cyclic voltammograms of the HER in deaerated 0.5 M H_2SO_4 (pH 0.40) were conducted. An O-ring seal was used to expose only the STM-imaged part of the sample to the electrolyte. The cyclic voltammogram sweep rate was 5 mV/s.

A SCE and a Pt mesh were used as reference and counter electrode, respectively.

2.4. Electrochemical Measurements in a Membrane Electrode Assembly (MEA). ***2.4.1. MEA Preparation.*** A 1 mL portion of $[Mo_3S_4]^{4+}$ solution (40 mM $[Mo_3S_4]^{4+}$ in 4 M H_2SO_4) was wet-impregnated on 160 mg of Carbot xc72 carbon black and dried. An ink was then prepared with 44 mg of the carbon-supported $[Mo_3S_4]^{4+}$, 0.1 mL of Nafion solution (5 wt % in a mixture of lower aliphatic alcohols and water), and 0.2 mL of methanol (99.99%). The ink was sonicated for 40 min, drop-cast on a 3.14 cm^2 graphite paper disk (Toray), and dried to create a gas diffusion electrode (GDE) with $[Mo_3S_4]^{4+}$.

The GDE with $[Mo_3S_4]^{4+}$ was hot pressed (130 °C and 32 bar for 5 min) together with a 117 Nafion membrane and a commercial Pt GDE (IRD Fuel Cell Technology), creating an MEA with a Pt GDE on one side and a $[Mo_3S_4]^{4+}$ GDE on the other side.

2.4.2. Electrochemical Measurements of the MEA. The MEA was tested in a fuel cell test setup, where prehumidified H_2 (99.9999%) was passed over the GDEs. All measurements were performed at room temperature, with a gas flow of 20 mL/min over both electrodes, and at a scan rate of 5 mV/s. The Pt GDE was used as both reference (effectively a NHE electrode) and counter electrode.

2.5. Scanning Tunneling Microscopy (STM). STM was performed using a Pico SPM instrument (Molecular Imaging Co., USA). Pt/Ir tips (80/20, Ø 0.25 mm) were prepared by electrochemical etching.[11] The sharpness of the tips was checked by recording HOPG images with atomic resolution. $[Mo_3S_4]^{4+}$/HOPG samples were characterized to single-molecule resolution by STM in air.

2.6. X-ray Photoelectron Spectroscopy (XPS). XPS was performed using a Perkin-Elmer surface analysis system (Physical Electronics Industries Inc., USA). Al Kα radiation (1486.6 eV) was used for excitation. High-resolution scans, with a total energy resolution of about 1.0 eV, were recorded with a pass energy of 25 eV, a step size of 0.2 eV, and 500 ms/step. Base pressure of the chamber was 10^{-10} Torr. Spectra were calibrated to C 1s at 284.5 eV.

3. Results and Discussion

3.1. Electrochemical Characterization of $[Mo_3S_4]^{4+}$ in a Fuel Cell Setup. ***3.1.1. Electrochemical Fuel Cell Behavior of Carbon-supported $[Mo_3S_4]^{4+}$ Multilayers.*** The $[Mo_3S_4]^{4+}$ were initially deposited on high surface area carbon (xc72), which allowed us to test the electrocatalytic activity in a MEA. The xc72 is a highly defected high surface area carbon and was chosen to anchor the $[Mo_3S_4]^{4+}$ to defects, eventually creating an MEA with a high dispersion of $[Mo_3S_4]^{4+}$. The MEA was tested in a fuel cell test setup, enabling testing for the activity of both the HER and the HOR (hydrogen oxidation reaction). One particular concern of a metal sulfide in an acidic environment (such as Nafion) is its irreversible oxidation at anodic potentials. However, $[Mo_3S_4]^{4+}$ showed no sign of irreversible oxidation at anodic potentials up to 1 V versus NHE in the initial electrochemical measurements, Figure 2A. This is in contrast to MoS_2, which is known to irreversibly oxidize at these potentials.[32,33] We did, however, notice a reversible oxidation feature at 0.73 V versus NHE that we assign to desorption and readsorption of the $[Mo_3S_4]^{4+}$. Cathodic desorption of the $[Mo_3S_4]^{4+}$ has previously been observed in an aqueous solution by Kristensen et al.[11] The fact that we observe a readsorption peak, located at 0.65 V versus NHE in Figure 2A, is most likely due to the slow diffusion of $[Mo_3S_4]^{4+}$ into the electrolyte

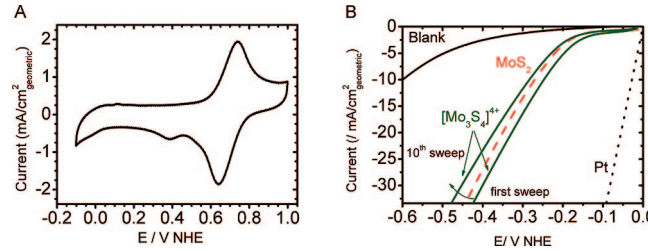

Figure 2. Electrochemical characterization of vulcan xc72-supported $[Mo_3S_4]^{4+}$ in a membrane electrode assembly. The potential is measured with respect to a Pt electrode that serves as both the reference and the counter electrode. (A) Cyclic voltammogram in the anodic region, showing a reversible oxidation feature at ca. 0.7 V. (B) Polarization curves in the cathodic region where hydrogen is evolved. The activity of $[Mo_3S_4]^{4+}$ is compared with a blank electrode only containing xc72, a sample with Pt, and a sample with MoS_2. Hydrogen was passed over both electrodes, and the scanrate was 5 mV/s.

(Nafion) where desorbed $[Mo_3S_4]^{4+}$ is maintained in close proximity to the electrode, unlike the case reported by Kristensen et al. on a sub-monolayer of $[Mo_3S_4]^{4+}$. The desorption/readsorption ($[Mo_3S_4]^{4+}$ mobility) scenario is furthermore consistent with our observations that the Nafion membrane used for this study turned green, the same color as $[Mo_3S_4]^{4+}$ in the H_2SO_4 solution. At anodic potentials we did not measure any evidence of the HOR; see Figure 2A. We did, however, find that hydrogen was evolved at low cathodic overpotentials (approximately −150 mV). A comparison of the overpotentials is shown in Figure 2B. It is noted that the $[Mo_3S_4]^{4+}$ overpotential is similar to that of nanoparticulate MoS_2.[27,28] It should also be noted that the current at high cathodic potentials decreases for every cathodic sweep, whereas the overpotential remains constant. This could be caused by dissolution or agglomeration of the clusters.

On the basis of the similarity in overpotentials for the HER, the $[Mo_3S_4]^{4+}$ appear to have an activation barrier for the HER comparable to that of the previously studied MoS_2 system. $[Mo_3S_4]^{4+}$ could thus be a promising electrocatalyst for the HER. However, in order to compare the two systems more directly, studies of well-defined $[Mo_3S_4]^{4+}$ samples with known quantity and dispersion are essential, as reported in the following section.

3.1.2. Electrochemical Preparation and STM Imaging of Carbon-supported $[Mo_3S_4]^{4+}$ Sub-monolayers on HOPG. The preparation of well-dispersed molecular scale catalytic units with minimal agglomeration is critical to all nanoscale materials studied. A significant challenge in the present work was the preparation of an electrode with a high loading of $[Mo_3S_4]^{4+}$ molecules while maintaining independent moieties. HOPG was chosen as the support material because (1) it is an atomically flat substrate suitable for high-resolution (i.e., atomic) mapping by STM and (2) it is electrochemically inert within the potential window under investigation. The strong two-dimensional bonding within the sheets of graphite and inherently low defect density results, however, in rather weak bonding with surface adsorbates, which are typically physisorbed only through van der Waals forces. STM imaging of drop-casted $[Mo_3S_4]^{4+}$ on freshly cleaved HOPG surface thus revealed significant agglomeration with large mounds of $[Mo_3S_4]^{4+}$ (images not shown). High $[Mo_3S_4]^{4+}$ surface mobility presumably results from weak interactions between the adsorbate and the pristine HOPG surface.

To prevent surface diffusion of the clusters, we electrochemically activated a freshly cleaved HOPG surface by an anodic pulse procedure previously developed.[31] Surface functional groups such as −OH, −C═O, and −COOH, which serve to

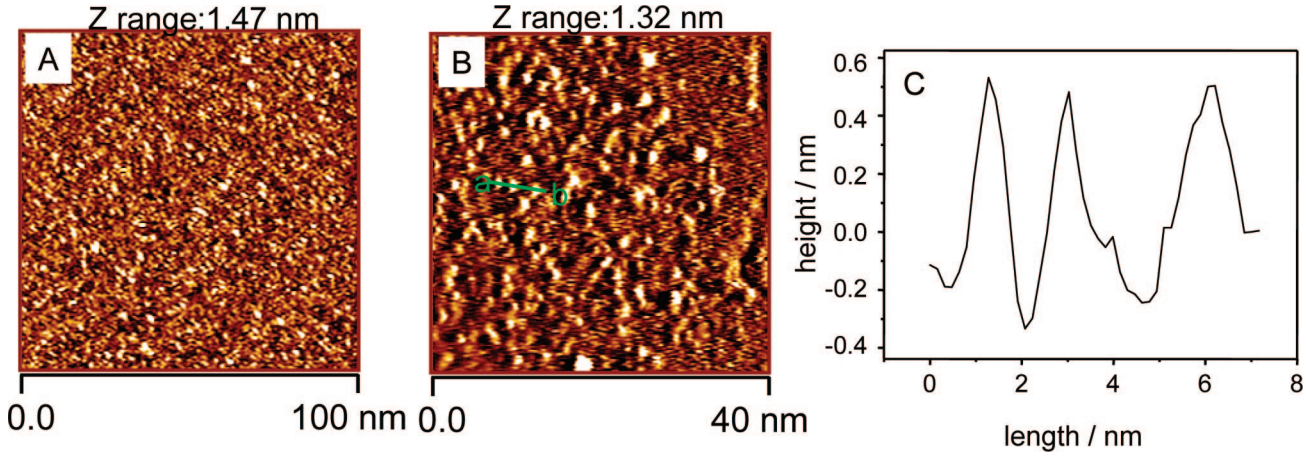

Figure 3. STM images (A and B) of HOPG-supported $[Mo_3S_4]^{4+}$. The coverage of the $[Mo_3S_4]^{4+}$molecule (most likely including ligands) on HOPG is about 1.0 ($\pm$0.1) $\times$ 10^{13} molecules/cm^2, corresponding to 1.6 ($\pm$0.2) $\times$ 10^{-11} mol/cm^2. Each molecule is ~2.0 ($\pm$0.5) nm in diameter from STM measurement, and an ideal close packed surface contains ~3.2 ($\pm$0.8) $\times$ 10^{13} molecules/cm^2. (A) Tunnelling current, I_t = 0.20 nA, V_{bias} = 0.90 V, *Z*-range = 1.47 nm. (B) Tunnelling current, I_t = 0.30 nA, V_{bias} = 0.80 V, *Z*-range = 1.32 nm. A typical cross section of the adsorbed clusters is shown in panel C, along the green line in panel B. The height is about 7.5−8.5 Å, and the length is in a range of 1.5−2.5 nm. Considering the contribution of anions around cation clusters, this value is close to a size for individual $[Mo_3S_4]^{4+}$ moieties, indicating that individual clusters are uniformly scatted on the activated HOPG surface.

anchor the $[Mo_3S_4]^{4+}$ (by electrostatic interaction or ligand substitution) as well as to improve surface hydrophilicity, could be introduced in this way.

Figure 3 shows STM images of this surface after drop-casting an aliquot of the aqueous $[Mo_3S_4]^{4+}/H_2SO_4$ solution. Only insignificant agglomeration is seen. Verifying the predominance of independently adsorbed $[Mo_3S_4]^{4+}$ (approximately 2 nm diameter, which includes the H_2O/SO_4^{2-} coordination shell), was a crucial step needed to directly correlate the structure and function of these molecular entities at the level of the single $[Mo_3S_4]^{4+}$-molecule catalyst. Furthermore, STM offered a quantitative measure of the surface coverage, which was determined to be 1.6 ($\pm$0.2) $\times$ 10^{-11} mol $[Mo_3S_4]^{4+}$/cm^2 HOPG, corresponding to a surface density of 1.0 ($\pm$0.1) $\times$ 10^{13} $[Mo_3S_4]^{4+}$-molecules/cm^2.

3.1.3. Electrocatalysis of the HER by a $[Mo_3S_4]^{4+}$ Sub-monolayer in a Three-electrode Cell: Electroatalytic Efficiency Per Single-molecule $[Mo_3S_4]^{4+}$. After STM imaging of the sub-monolayer of $[Mo_3S_4]^{4+}$ on the activated HOPG had established that the sample indeed consisted of a sub-monolayer of independent molecules, exactly the same sample was electrochemically characterized in a three-electrode cell. Figure 4 shows a series of CVs. Hydrogen is evolved in the initial sweep at potentials negative of −0.2 V versus NHE. This is the same region where the HER on the high surface area carbon-supported $[Mo_3S_4]^{4+}$ was observed. The slow scanrate of 5 mV/s ensured that the influence of transport limitations was small, as confirmed by observing reasonable Tafel slopes (mV/dec) and a continually increasing current at high overvoltages. The Tafel plot in the inset of Figure 4 yields an exchange current density of 2.2 $\times$ 10^{-7} A/cm$^2_{geometric}$ with a Tafel slope of 120 mV/dec.

The combination of electrochemistry and STM, resolved to the level of the single molecule, enables direct conversion to the turnover frequency per molecule. We have previously exploited this combination to assess the number of redox metalloproteins on (bio)electrochemical surfaces.[27,28,34,35] The turnover frequency per $[Mo_3S_4]^{4+}$ molecule was found to be 0.07 s^{-1}. We do not know the exact number of active sites per $[Mo_3S_4]^{4+}$ molecule, but this value is comparable to or even better than the turnover frequency of 0.02 s^{-1} reported for a single site on the edge of MoS_2 nanoparticles.[27] The turnover frequency is, however, smaller than for the turnover frequency

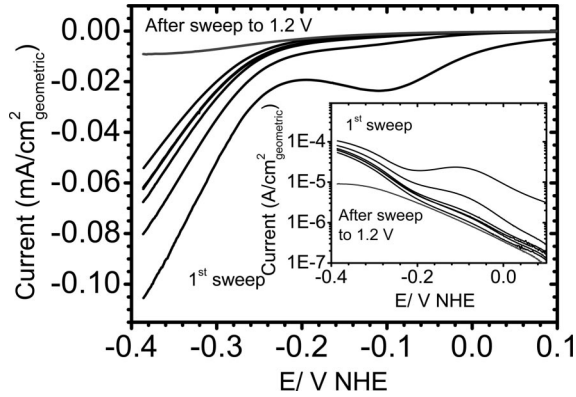

Figure 4. Electrochemical characterization of the sub-monolayer of $[Mo_3S_4]^{4+}$ on HOPG showing subsequent negative potential sweeps. Main: Polarization curve in the cathodic region showing hydrogen evolution. The decrease in activity from sweep-to-sweep is most likely due to cathodic desorption of the clusters, as observed at −0.1 V vs NHE. After a final anodic sweep to high potentials of +1.2 V vs NHE, the clusters completely desorb, and the flat signal observed on the final, subsequent cathodic sweep pertains to that of the inert HOPG substrate. Inset: the corresponding Tafel plot. The scanrate was 5 mV/s.

per atom of the archetypical HER catalyst[24] (Pt, Pd). In addition, there are many more active atoms on the Pt metal surface than $[Mo_3S_4]^{4+}$ even in a densely packed monolayer. The per molecule activity is, on the other hand, larger compared with commonly considered nonprecious metal HER catalysts,[24] such as Ni, Cu, or W.

A reduction peak is seen around −0.12 V versus NHE in the first sweep. This peak could be due to cathodic desorption of $[Mo_3S_4]^{4+}$ as previously proposed,[11] but no conclusive evidence exist on the exact nature of this peak.

3.2. XPS Data. Spectroscopic evidence of $[Mo_3S_4]^{4+}$ on the surface is crucial, as this ensures that catalytic activity of the $[Mo_3S_4]^{4+}$ molecules is addressed and not that of a contaminant or an oxidized Mo species. XPS holds clues to such assessments. XPS data from both a bulk sample with multilayers of $[Mo_3S_4]^{4+}$, to verify that the $[Mo_3S_4]^{4+}$ molecules have the expected electronic structure, and from sub-monolayer $[Mo_3S_4]^{4+}$, evaluated for catalytic activity, are compared below.

3.2.1. Bulk $[Mo_3S_4]^{4+}$. XPS data of $[Mo_3S_4]^{4+}$ immobilized on "activated" HOPG offers important insight in the electronic

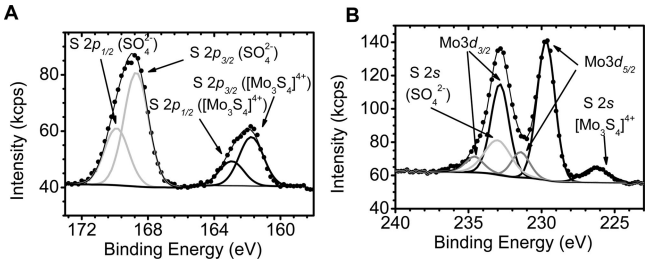

Figure 5. XPS spectra of multilayers of $[Mo_3S_4]^{4+}$ on HOPG. (A) The S 2p region of SO_4^{2-} and $[Mo_3S_4]^{4+}$. (B) The S 2s of SO_4^{2-} and $[Mo_3S_4]^{4+}$, and the Mo 3d region of $[Mo_3S_4]^{4+}$.

states of the Mo- and S-atoms of the active catalyst molecule. As a reference, XPS of bulk $[Mo_3S_4]^{4+}/SO_4^{2-}$ was first recorded; see Figure 5. The deconvoluted Mo 3d, S 2s, and S 2p regions of the XPS spectra of this film are shown in Figure 5. Niemantsverdriet et al,[36] reported XPS of $K_5[Mo_3S_4(CN)_9]\cdot 3KCN\cdot 4H_2O$, which contains the same $Mo_3S_4^{4+}$ core, albeit with cyano ligands and potassium cations rather than aqua ligands and sulfate anions. The sulfate anion present in our system gives additional sulfur lines. At first glance these appear to distinguish our spectra from those of ref 36, but peak deconvolution discloses that the two $[Mo_3S_4]^{4+}$ films are, in fact, spectroscopically similar (see Table 1).

The energy window shown in Figure 5B, containing overlapping Mo 3d and S 2s transitions, has been deconvoluted into six distinct peaks: S 2s of $[Mo_3S_4]^{4+}$, S 2s of SO_4^{2-}, and two Mo-components leading to two sets of Mo 3d doublets, with a major (84%) and a minor component (16%, shifted 1.75 eV positive). The S 2p lines of $[Mo_3S_4]^{4+}$ and SO_4^{2-}, shown in Figure 5A, are readily distinguished from one another. The lower intensity broad peak at 233.1 eV was assigned to the S 2s line in SO_4^{2-}, consistent with ref 37 and verified by XPS experiments in which H_2SO_4 was drop-cast alone onto an HOPG surface (data not shown). This line, not present in the system studied by Niemantsverdriet et. al,[36] coincides with the Mo $3d_{3/2}$ line that they assign to $[Mo_3S_4]^{4+}$. Deconvolution of the peaks was undertaken using Gaussian peak shapes and the following data fitting constraints: splitting: S 2p = 1.19 eV, Mo 3d = 3.15 eV; intensity ratios: Mo $3d_{3/2}$ = 2/3 × Mo $3d_{5/2}$, S $2p_{1/2}$ = 0.5 × S $2p_{3/2}$, S 2s($[Mo_3S_4]^{4+}$)/S 2s(SO_4^{2-}) = S 2p($[Mo_3S_4]^{4+}$)/S 2p(SO_4^{2-}), and finally, the Gaussian peak full width half-maximum (fwhm) was fixed for the same species in the same energy window (e.g., fwhm Mo $3d_{5/2}$ = fwhm Mo $3d_{3/2}$). Apart from the S 2s and S 2p lines assigned to SO_4^{2-}, and the Mo *3*d doublet of the minor Mo-component, our data and that of ref 36 are quite similar. The Mo $3d_{5/2}$ line at 229.70 eV indicates that molybdenum is in the formal 4+ state,[32] whereas the S^{2-} ligands of $[Mo_3S_4]^{4+}$, observed as the S 2p line at 161.76 eV, is close to the S^{2-} ligands in MoS_2. Only small differences between the spectra reported with thick $Mo_3S_4^{4+}$ film and those in ref 36 are thus found, presumably caused by the different ligands and counterions. We shall discuss the nature of the minor Mo-component in Section 3.2.2.

3.2.2. XPS: Bulk versus Sub-monolayer $[Mo_3S_4]^{4+}$. XPS of the sub-monolayer $[Mo_3S_4]^{4+}$ on activated HOPG was recorded, and the survey spectra (not shown) showed no evidence of contamination. Figure 6 shows the deconvoluted S 2p spectrum (Figure 6A) that corresponds well with that of bulk $[Mo_3S_4]^{4+}$. The S 2p peak of SO_4^{2-} is of lower intensity (relative to the 2p of $[Mo_3S_4]^{4+}$) than for bulk $[Mo_3S_4]^{4+}$, this being due to the difference in film preparation. Excess drop-casted reagent (1.8 mM $[Mo_3S_4]^{4+}$ in 0.4 M H_2SO_4) was not thoroughly rinsed off in bulk $[Mo_3S_4]^{4+}$ film preparation, whereas this was the case for sub-monolayer $[Mo_3S_4]^{4+}$. However, a more notable difference in the XPS is observed for the deconvoluted Mo 3d and S 2s regions. Compared to the bulk case, two sets of Mo 3d doublets are now easily distinguished; the major (59%) doublet at 230.14 and 233.29 eV line up with the Mo $3d_{5/2}$ and Mo $3d_{3/2}$ of bulk $[Mo_3S_4]^{4+}$, whereas the minor (41%) set of peaks at 232.41 and 235.56 eV are shifted by 2.27 eV toward higher binding energies. The intensity of the major set of peaks relative to the minor set of peaks is significantly lower in this sample compared to the bulk sample. However, we find that the intensity ratio between the Mo 3d peaks (major + minor component) and the S 2p peak at 162.44 eV, all related to $[Mo_3S_4]^{4+}$, is very similar to the bulk case (Figure 5). This shows that there is no loss of sulfur in the sub-monolayer $[Mo_3S_4]^{4+}$.

The minor, high binding energy Mo 3d-component we observe in both the sub-monolayer and multilayer sample is not likely due to oxidation of Mo^{4+} to Mo^{6+} (such as in MoO_3),[32,33] or due to replacement of S^{2-} ligands in the cluster by O^{2-}, studied by Shibahara et al. for $[Mo_3O_{4-n}S_n]^{4+}$ (n = 0−4) clusters.[38] This is because we obtain near identical sulfur-to-Mo ratio in $[Mo_3S_4]^{4+}$ for the sub-monolayer and multilayer samples, although the ratio between major and minor Mo 3d component is drastically different. We instead assign the minor Mo 3d component to distinct differences in local environment of Mo atoms in the adsorbed $[Mo_3S_4]^{4+}$ structures. Such differences can arise from (1) lower coordination of the clusters, giving rise to a lower final state screening in XPS; (2) a difference in number (concentration) of SO_4^{2-} counterions, or (3) O adsorption on the clusters. The lower relative concentration of the minor Mo 3d high binding energy component in the multilayer $[Mo_3S_4]^{4+}$ sample compared to the sub-monolayer sample is likely due to the fact that such local environment differences only are found at the outmost surface layer(s) in the multilayer case.

3.2.3. XPS: Sub-monolayer $[Mo_3S_4]^{4+}$ after Cyclic Voltammetry. The loss in catalytic activity of $[Mo_3S_4]^{4+}$ on HOPG after voltammetric sweeps was also investigated by XPS; see Figure 7. The S 2p and S 2s peaks that correspond to SO_4^{2-} were still strongly visible in the XPS spectra recorded subsequent to cyclic voltammetry. The Mo 3d and S 2p peaks assigned to $[Mo_3S_4]^{4+}$, however, decreased significantly. Little or no Mo is left on the surface.

4. Conclusions and Perspectives

$[Mo_3S_4]^{4+}$-type clusters have long been known as a crucial part of polynuclear Mo−S chemistry. $[Mo_3S_4]^{4+}$ is one example of a prototype cluster in a broader class of $[Mo_3MS_4]^{n+}$ cluster types with a variety of heterometal ions. Catalytic $[Mo_3MS_4]^{4+}$-based activity in hydrodesulfurization, N−N cleavage of hydrazine, and other organic chemical reactions are notable.

We have introduced $[Mo_3S_4]^{4+}$ as a novel prototype catalyst in heterogeneous catalysis, specifically in the electrocatalytic evolution of hydrogen on different graphite supports of direct relevance to fuel cell electrode surfaces. $[Mo_3S_4]^{4+}$ immobilized on electrode surfaces by electrochemical pulse pretreatment to create molecular surface functionalities were found, first to act as an efficient electrocatalyst for the HER in the electrochemical fuel cell-like environment. The $[Mo_3S_4]^{4+}$-based catalytic efficiency, compares well with the recently reported high electrocatalytic efficiency of identified MoS_2 edge surface sites. The observed catalysis displayed some instability on successive potential scanning, but this was largely due to desorption of the catalyst molecules from the surface rather than decomposi-

TABLE 1: XPS Data for a sub-monolayer of $[Mo_3S_4]^{4+}$ and a "thick", multi-layer $[Mo_3S_4]^{4+}$ film deposited on HOPG

		sub-monolayer		multilayer		
assigned species	spectral line	fwhm[a]	binding energy (eV)[a]	fwhm[a]	binding energy (eV)[a]	binding energy (eV)[b]
$[Mo_3S_4]^{4+}$	S $2p_{3/2}$	2.36	162.44 ± 0.1	1.74	161.76 ± 0.1	~161.6
$[Mo_3S_4]^{4+}$	S $2p_{1/2}$	2.36	163.63 ± 0.1	1.74	162.95 ± 0.1	~162.6
$[Mo_3S_4]^{4+}$	S 2s	1.14	226.68 ± 0.1	2.13	226.29 ± 0.1	~226.0
$[Mo_3S_4]^{4+}$	Mo $3d_{5/2}$	2.09	230.14 ± 0.1	1.46	229.70 ± 0.1	~229.3
$[Mo_3S_4]^{4+}$	Mo $3d_{3/2}$	2.09	233.29 ± 0.1	1.46	232.85 ± 0.1	~232.5
SO_4^{2-}	S $2p_{3/2}$	2.36	168.45 ± 0.55	1.74	168.71 ± 0.1	
SO_4^{2-}	S $2p_{1/2}$	2.36	169.64 ± 0.55	1.74	169.90 ± 0.1	
SO_4^{2-}	S 2s	1.14	234.80 ± 0.37	2.13	232.99 ± 0.1	
$[Mo_3S_4]^{4+}$ minor	Mo $3d_{5/2}$	2.09	232.41 ± 0.1	1.46	231.44 ± 0.1	
$[Mo_3S_4]^{4+}$ minor	Mo $3d_{3/2}$	2.09	235.56 ± 0.1	1.46	234.59 ± 0.1	

[a] This work. [b] Reference 36 (values read off raw spectra).

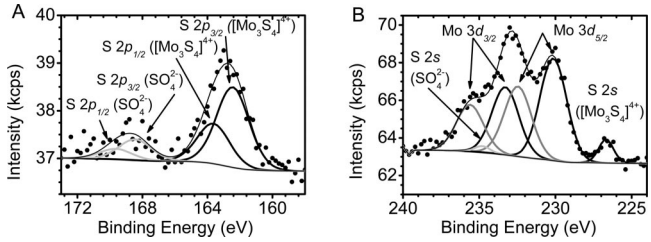

Figure 6. XPS spectra of a sub-monolayer of $[Mo_3S_4]^{4+}$ on HOPG. (A) The S 2p region of $SO_4^{2-}$and $[Mo_3S_4]^{4+}$. (B) The S 2s of $SO_4^{2-}$and $[Mo_3S_4]^{4+}$ and the Mo 3d region of $[Mo_3S_4]^{4+}$.

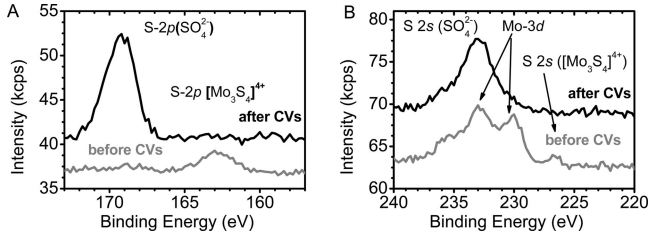

Figure 7. XPS spectra of a submonolayer of $[Mo_3S_4]^{4+}$ on HOPG before (Gray) and after electrochemical measurements (Black). (A) The S 2p region of $SO_4^{2-}$and $[Mo_3S_4]^{4+}$. (B) The S 2s of SO_4^{2-} and $[Mo_3S_4]^{4+}$ and the Mo 3d region of $[Mo_3S_4]^{4+}$.

tion and can be improved upon further optimization of the immobilization procedure. Second, the unique combination of electrochemistry and STM, resolved to the level of the single molecule, could directly convert the catalytic efficiency to the single-molecule scale. In this way the electrocatalytic activity per molecule was found to be comparable with that of the edge sites of MoS_2. Through the multifarious and tunable $[Mo_3S_4]^{4+}$-unit, extendable to the whole class of heterometallic cluster compounds, these observations have opened novel routes to a new and potentially powerful class of interfacial electrocatalysts useable for one of the altogether most important electrochemical processes, the electrochemical HER reaction.

Our study rests on a comprehensive approach. In addition to cyclic voltammetry, chemical surface immobilization and electrochemical in situ STM, we have characterized the electronic properties of the $[Mo_3S_4]^{4+}$ by XPS, used to investigate both bulk and sub-monolayers of $[Mo_3S_4]^{4+}$. XPS of macroscopic $[Mo_3S_4]^{4+}/SO_4^{2-}$ film samples showed the expected majority of $3d_{5/2}$ and $3d_{3/2}$ spectral peak features for Mo in the formal 4+ oxidation state and a minority of $3d_{5/2}$ and $3d_{3/2}$ spectral peak features for Mo at higher binding energies as well as the 2s, $2p_{3/2}$, and $2p_{1/2}$ S signals. In addition, corresponding signals of the SO_4^{2-} anion were observed. These data showed, interestingly, that the $[Mo_3S_4]^{4+}$-core structure is similar to that for a related but different Mo-complex studied by Niemantsverdriet and associates.[36]

The sub-monolayers of $[Mo_3S_4]^{4+}$ were found to differ from $[Mo_3S_4]^{4+}$ in the bulk state. The Mo 3d peaks at higher binding energies were more pronounced than in the bulk sample, indicating that part of the Mo-atoms in the $[Mo_3S_4]^{4+}$ are present in a different local environment. We cannot presently offer a precise rationale for this difference, but the mixed-valence nature of $[Mo_3S_4]^{4+}$ in the (strongly) adsorbed state can be a rationale for the observed electrocatalytic activity. Such "tunable" electronic properties are often prerogatives for efficient electronic transmission in chemical and biological charge transfer processes.

XPS finally substantiated that $[Mo_3S_4]^{4+}$ desorption is the primary cause of the apparent gradual catalytic deactivation on successive voltammetric scanning.

In conclusion, a new class of polynuclear Mo−S cluster-based catalyst has been found to show very high per-molecule catalytic efficiency in the electrochemical HER on carbon-based electrode surfaces. The prototype representative, that is, the incomplete cubane-type cluster, $[Mo_3S_4]^{4+}$, has been in focus but is otherwise representative of the broader class of homologous heterometallic cubane-type clusters, $[Mo_3MS_4]^{4+}$. Once the observed electrocatalytic stability issue has been rectified, this class may offer new prospects as a broad and electronically versatile class of electrocatalysts in practical working environments.

Acknowledgment. This work was supported by the National Research Foundation (CINF), the Danish Research Council through FTP and NABIIT. T.F.J. acknowledges the H.C. Ørsted Postdoctoral Fellowship from the Technical University of Denmark, K.A. acknowledges financial support from The Wenner-Gren Foundations, and J.B. acknowledges support from the Danish Strategic Research Council.

References and Notes

(1) Steele, B. C. H.; Heinzel, A. *Nature* **2001**, *414*, 345–352.
(2) Scott, T. A.; Berlinguette, C. P.; Holm, R. H.; Zhou, H. C. *Proc. Natl. Acad. Sci. U.S.A.* **2005**, *102*, 9741–9744.
(3) Lee, S. C.; Holm, R. H. *Chem. Rev.* **2004**, *104*, 1135–1157.
(4) Rao, P. V.; Holm, R. H. *Chem. Rev.* **2004**, *104*, 527–559.
(5) Hernandez-Molina, R.; Sokolov, M. N.; Sykes, A. G. *Acc. Chem. Res.* **2001**, *34*, 223–230.
(6) Shibahara, T.; Kuroya, H. *Polyhedron* **1986**, *5*, 357–361.
(7) Takei, L.; Dohki, K.; Kobayashi, K.; Suzuki, T.; Hidai, M. *Inorg. Chem.* **2005**, *44*, 3768–3770.
(8) Wakabayashi, T.; Ishii, Y.; Ishikawa, K.; Hidai, M. *Angew. Chem.-Int. Ed. Engl.* **1996**, *35*, 2123–2124.
(9) Taniguchi, M.; Imamura, D.; Ishige, H.; Ishii, Y.; Murata, T.; Hidai, M.; Tatsumi, T. *J. Catal.* **1999**, *187*, 139–150.
(10) Wakabayashi, T.; Ishii, Y.; Murata, T.; Mizobe, Y.; Hidai, M. *Tetrahedron Lett.* **1995**, *36*, 5585–5588.

(11) Kristensen, J.; Zhang, J. D.; Chorkendorff, I.; Ulstrup, J.; Ooi, B. L. *Dalton Transactions* **2006**, 3985–3990.

(12) Armstrong, F. A. *Curr. Opin. Chem. Biol.* **2005**, *9*, 110–117.

(13) Vincent, K. A.; Parkin, A.; Armstrong, F. A. *Chem. Rev.* **2007**, *107*, 4366–4413.

(14) Hammerich, O., Ulstrup, J., Eds.; *Bioinorganic Electrochemistry*; Springer: Dordrecht, 2008; pp xiv, 310.

(15) Shigehara, K.; Anson, F. C. *J. Phys. Chem.* **1982**, *86*, 2776–2783.

(16) Jiang, R.; Dong, S. *Electrochim. Acta* **1990**, *35*, 1227–1232.

(17) Younathan, J. N.; Wood, K. S.; Meyer, T. J. *Inorg. Chem.* **1992**, *31*, 3280–3285.

(18) Lei, J.; Ju, H.; Ikeda, O. *Electrochim. Acta* **2004**, *49*, 2453–2460.

(19) De Groot, M. T.; Merkx, M.; Wonders, A. H.; Koper, M. T. M. *J. Am. Chem. Soc.* **2005**, *127*, 7579–7586.

(20) Abild-Pedersen, F.; Greeley, J.; Studt, F.; Rossmeisl, J.; Munter, T. R.; Moses, P. G.; Skulason, E.; Bligaard, T.; Nørskov, J. K. *Phys. Rev. Lett.* **2007**, *99*, 016105.

(21) Bligaard, T.; Nørskov, J. K.; Dahl, S.; Matthiesen, J.; Christensen, C. H.; Sehested, J. *J. Catal.* **2004**, *224*, 206–217.

(22) Dresselhaus, M. S.; Thomas, I. L. *Nature* **2001**, *414*, 332–337.

(23) Parsons, R. *Trans. Faraday Soc.* **1958**, *54*, 1053–1063.

(24) Nørskov, J. K.; Bligaard, T.; Logadottir, A.; Kitchin, J. R.; Chen, J. G.; Pandelov, S.; Stimming, U. *J. Electrochem. Soc.* **2005**, *152*, J23.

(25) Greeley, J.; Nørskov, J. K.; Kibler, L. A.; El-Aziz, A. M.; Kolb, D. M. *ChemPhysChem* **2006**, *7*, 1032–1035.

(26) Greeley, J.; Jaramillo, T. F.; Bonde, J.; Chorkendorff, I. B.; Nørskov, J. K. *Nat. Mater.* **2006**, *5*, 909–913.

(27) Jaramillo, T. F.; Jørgensen, K. P.; Bonde, J.; Nielsen, J. H.; Horch, S.; Chorkendorff, I. *Science* **2007**, *317*, 100–102.

(28) Hinnemann, B.; Moses, P. G.; Bonde, J.; Jørgensen, K. P.; Nielsen, J. H.; Horch, S.; Chorkendorff, I.; Nørskov, J. K. *J. Am. Chem. Soc.* **2005**, *127*, 5308–5309.

(29) Sakane, G.; Shibahara, T. *Inorg. Synth.* **2002**, *33*, 144–149.

(30) Martinez, M.; Ooi, B. L.; Sykes, A. G. *J. Am. Chem. Soc.* **1987**, *109*, 4615–4619.

(31) Zhang, J. D.; Chi, Q. J.; Dong, S. J.; Wang, E. K. *Bioelectrochem. Bioenerget.* **1996**, *39*, 267–274.

(32) Bonde, J.; Moses, P. G.; Jaramillo, T. F.; Nørskov, J. K.; Chorkendorff, I. *Faraday Discuss.* **2008**, DOI: 10.1039/b803857k.

(33) Jaegermann, W.; Schmeisser, D. *Surf. Sci.* **1986**, *165*, 143–160.

(34) Chi, Q. J.; Zhang, J. D.; Jensen, P. S.; Christensen, H. E. M.; Ulstrup, J. *Faraday Discuss.* **2006**, *131*, 181–195.

(35) Chi, Q. J.; Farver, O.; Ulstrup, J. *Proc. Natl. Acad. Sci. U. S. A.* **2005**, *102*, 16203–16208.

(36) Muijsers, J. C.; Weber, T.; vanHardeveld, R. M.; Zandbergen, H. W.; Niemantsverdriet, J. W. *J. Catal.* **1995**, *157*, 698–705.

(37) Wagner, C. D., Naumkin, A. V., Kraut-Vass, A. Allison, J. W. , Powerll, C. J.; Rumble Jr., J. R., NIST X-Ray Photoelectron Spectroscopy Database, Standard Reference Database 20, Ver. 3.4; 2008. http://srdata.nist.gov/xps.

(38) Shibahara, T.; Tsuru, H.; Kuroya, H. *Inorg. Chim. Acta* **1988**, *150*, 167–168.

JP802695E